A Novel Method to Quantify Contribution of Channels and Transporters to Membrane Potential Dynamics

Chae Young Cha,[†] Yukiko Himeno,[‡] Takao Shimayoshi,[§] Akira Amano,[†] and Akinori Noma[†*]
[†]Biosimulation Project, Faculty of Bioinformatics, Ritsumeikan University, Kusatsu City, Japan; [‡]Biosimulation Project, Graduate School of Medicine, Kyoto University, Kyoto, Japan; and [§]Advanced Scientific Technology and Management Research Institute of Kyoto, Kyoto, Japan

ABSTRACT The action potential, once triggered in ventricular or atrial myocytes, automatically proceeds on its time course or is generated spontaneously in sinoatrial node pacemaker cells. It is induced by complex interactions among such cellular components as ion channels, transporters, intracellular ion concentrations, and signaling molecules. We have developed what is, to our knowledge, a new method using a mathematical model to quantify the contribution of each cellular component to the automatic time courses of the action potential. In this method, an equilibrium value, which the membrane potential is approaching at a given moment, is calculated along the time course of the membrane potential. The calculation itself is based on the time-varying conductance and the reversal potentials of individual ion channels and electrogenic ion transporters. Since the equilibrium potential moves in advance of the membrane potential change, we refer to it as the lead potential, V_L. The contribution of an individual current was successfully quantified by comparing dV_L/dt before and after fixing the time-dependent change of a component of interest, such as the variations in the open probability of a channel or the turnover rate of an ion transporter. In addition to the action potential, the lead-potential analysis should also be applicable in all types of membrane excitation in many different kinds of cells.

INTRODUCTION

The membrane potential (V_m) of excitable cells shows active changes, such as generation of action potentials or spontaneous oscillations, which are automatically generated by complex interactions among multiple cellular components including ion channels, transporters, ion concentrations, signaling molecules, or even by V_m itself. Electrophysiological studies have been conducted to elucidate the ionic mechanisms underlying these active V_m changes. A central problem in cardiac physiology has been to determine which cellular component is responsible for slow diastolic depolarization in sinoatrial (SA) node cells and for repolarization of the long-lasting ventricular action potential.

The contribution of each cellular component is difficult to measure with conventional experimental approaches that simply record changes in V_m or current size by modifying a component of interest. The difficulty arises because modification of a specific channel or transporter alters the activity of other channels or transporters secondarily via changes of V_m or ion concentrations. Therefore, only a qualitative inference can be drawn from the multiple layers of sequential events induced by modifying a given component. To overcome the experimental limitations, simulation studies have been attempted using mathematical models based on experimental findings. These models allow examination of modal shifts in the system behavior by modifying parameters of cellular components (1–4), stability of the system (3,4), and/or sensitivity of related parameters (5,6). However, it is difficult to estimate the contribution of each component quantitatively from these analyses because of the complexity underlying cardiac membrane excitation.

In this article, we propose what we believe to be a new analytic method, which we refer to as lead-potential analysis, to quantify the contribution of each cellular component to automatic changes in V_m. Our method could be used, for example, to determine the slow diastolic depolarization in the SA node or the long-plateau repolarization of the ventricular action potential. Using this method, a theoretical equilibrium potential (lead potential, V_L) is calculated while leaving the time course of V_m intact. The contribution of a given component is evaluated from modification of dV_L/dt induced by eliminating the time-dependency of the component.

The theoretical background is presented, and then the method is applied to SA node cells and ventricular myocytes as representative cardiac cell models.

METHODS

Definition of the lead potential (V_L)

We will derive an equilibrium value of V_m, which V_m tends to approach at a given time of observation (t_{ob}). We aim at expressing the membrane as a minimum linear electrical circuit in Fig. 1 *B*.

The temporal change of V_m is described with a fundamental equation in the absence of any extra current and spatial variation of V_m within a single cell,

$$\frac{dV_m}{dt} = -\frac{I_m}{C_m}, \quad (1)$$

where C_m is the whole cell membrane capacitance, and I_m is the sum of membrane currents through all ion channels and electrogenic transporters in a single cell. In most mathematical models, a current of channel X (I_X) is described by Ohm's law,

Submitted May 8, 2009, and accepted for publication August 6, 2009.

*Correspondence: noma@sk.ritsumei.ac.jp

Editor: Francisco Bezanilla.

0006-3495/09/12/3086/9 $2.00

doi: 10.1016/j.bpj.2009.08.060

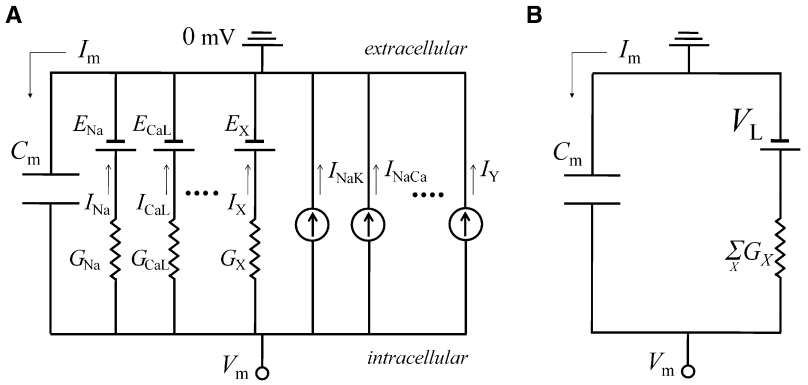

FIGURE 1 Equivalent electrical circuit of the cell membrane. (*A*) An equivalent circuit for the membrane electrical behavior expressed by Eq. 5. C_m, membrane capacitance; E_X, reversal potential for a channel X; I_Y, current through transporter Y; I_m, total membrane current. (*B*) A reduced circuit equivalent to Eq. 7.

$$I_X = g_{max} \times p(o) \times (V_m - E_{rev}) \quad (2)$$

or the Goldman-Hodgkin-Katz (GHK) current equation with a constant field approximation,

$$I_X = p_{max} \times p(o) \times \frac{V_m z_s^2 F^2}{RT} \frac{[S]_i - [S]_o \exp(-z_s F V_m/RT)}{1 - \exp(-z_s F V_m/RT)}, \quad (3)$$
$$= p_{max} \times p(o) \times f(V_m)$$

where g_{max} and p_{max} (which are defined as constants) are the maximum conductance and permeability, respectively. [S] is the concentration of ion S, and F, R, T, and z_s are the usual thermodynamic parameters. The value $p(o)$ is the open probability of a channel, which is determined by V_m- and/or ligand-dependent gating, pore-blocking, or unspecified mechanisms underlying the rectifying properties of ion channels. E_{rev} is a reversal potential for the channel in Eq. 2, and $f(V_m)$ represents the nonlinear part of the GHK equation in Eq. 3.

The following arguments are made at the moment of observation ($t = t_{ob}$). Since the electric elements are assumed to be linear, $f(V_m)$ is expressed as

$$f(V_m) = f'(V_m) \times (V_m - E), \quad (4)$$

where E is the value of intersection of the tangential line with the voltage axis. Then, all the channel currents can be expressed in the common form of $G_X \times (V_m - E_X)$, where

$$G_X = g_{max} \times p(o)$$

in Eq. 2, and

$$G_X = p_{max} \times p(o) \times f'(V_m)$$

in Eq. 3.

Thus, Eq. 1 is described as

$$\frac{dV_m}{dt} = -\frac{1}{C_m}\left(\sum_X G_X(V_m - E_X) + \sum_Y I_Y\right), \quad (5)$$

where X and Y are labels for a channel current and an ion transporter current, respectively. Equation 5 is equivalent to a linear electrical circuit shown in Fig. 1 *A*. An individual channel is expressed with one battery (E_X) and one conductance (G_X), and each transporter is represented by a current source (I_Y). C_m is assumed to be constant. Equation 5 can be rearranged as

$$\frac{dV_m}{dt} = -\frac{1}{C_m}\left(\sum_X G_X(V_m - E_X) + \sum_Y I_Y\right)$$
$$= -\frac{1}{C_m}\left(V_m \sum_X G_X - \sum_X G_X E_X + \sum_Y I_Y\right) \quad (6)$$
$$= -\frac{\sum_X G_X}{C_m}\left(V_m - \frac{\sum_X G_X E_X - \sum_Y I_Y}{\sum_X G_X}\right)$$

Then, Eq. 6 is described as

$$\frac{dV_m}{dt} = -\frac{1}{\tau}(V_m - V_L), \quad (7)$$

where

$$V_L = \frac{\sum_X G_X E_X - \sum_Y I_Y}{\sum_X G_X}, \quad (8)$$

$$\tau = \frac{C_m}{\sum_X G_X}. \quad (9)$$

Then, if we consider V_m as a free variable, Eq. 7 corresponds to Fig. 1 *B*. Therefore, V_m tends to approach an equilibrium value, V_L, with a time constant τ at each time point. Fig. 2 shows the temporal changes of V_L and V_m during an action potential in the SA node cell model (7) and

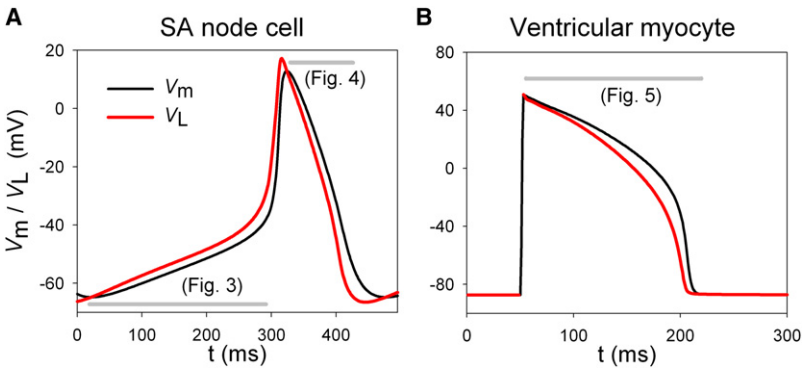

FIGURE 2 Time-dependent changes of V_L (*red*) and V_m (*black*) in the SA node cell model (*A*) and ventricular myocyte model (*B*). The period for current injection was excluded from calculation of V_L in panel *B* (50–52 ms). The gray bars indicate the time spans analyzed in Figs. 3–5.

ventricular myocyte model (8) obtained by calculating Eq. 8 at every moment. As V_L leads changes of V_m in advance, we refer to it as the lead potential. Note that V_L crosses V_m only when $dV_m/dt = 0$.

Estimation of contributions of ion channels and transporters to the automaticity of V_m

According to Fig. 1 *B* and Eq. 7, the automatic change of V_m is driven by the time-dependent change in V_L, and τ represents the passive property of the membrane. Therefore, the membrane automaticity can be expressed in terms of dV_L/dt with complete exclusion of τ:

$$\frac{dV_L}{dt} = \frac{\left(\sum_X \dot{G}_X E_X + \sum_X G_X \dot{E}_X - \sum_Y \dot{I}_Y\right)\sum_X G_X - \left(\sum_X G_X E_X - \sum_Y I_Y\right)\sum_X \dot{G}_X}{\left(\sum_X G_X\right)^2}. \quad (10)$$

Here, we will calculate the extent to which a component of interest affects dV_L/dt. Toward this end, we determine dV_{L_Fix}/dt after eliminating the time-dependent change of the component of interest (i.e., $\dot{G}_i = 0$, $\dot{E}_i = 0$, or $\dot{I}_i = 0$), leaving all the other components intact. We refer to this process of eliminating the time-dependent change as fixing. For example, when we fix G_i, we set $\dot{G}_i = 0$ in Eq. 10:

$$\frac{dV_{L\_Fix}}{dt} = \frac{\left(\sum_{X\neq i} \dot{G}_X E_X + \sum_X G_X \dot{E}_X - \sum_Y \dot{I}_Y\right)\sum_X G_X - \left(\sum_X G_X E_X - \sum_Y I_Y\right)\sum_{X\neq i} \dot{G}_X}{\left(\sum_X G_X\right)^2}. \quad (11)$$

The relative contribution, r_c, is defined as

$$r_c = \frac{\frac{dV_L}{dt} - \frac{dV_{L\_Fix}}{dt}}{\frac{dV_L}{dt}}\left(\text{when}\frac{dV_L}{dt} \neq 0\right), \quad (12)$$

and r_c satisfies the equation

$$\sum r_c = 1 \text{ for all components.} \quad (13)$$

An r_c of positive sign means that a component is operating to incline dV_L/dt in the same direction as the control dV_L/dt. On the other hand, an r_c of negative sign means that a component interferes with the change of V_L by inclining dV_L/dt in the opposite direction. If a component is entirely responsible for dV_L/dt, dV_{L_Fix}/dt is 0 and r_c equals 1.

Application to cell models

In this study, the temporal changes of r_c were calculated for $p(o)$, $f'(V_m)$, E_X, and I_Y. We confirmed that Eq. 13 was satisfied with a precision of 10^{-4}, that is, the sum of r_c became 1 at every moment (not shown). For physiological interest, we showed r_c obtained by fixing $p(o)$ for ion channels, or I_Y for transporters in Figs. 3–5. For the rest of the components, the time average of r_c was given in Table 1. The sum of r_c for E_X (E_{rev} in Eq. 2 and E in Eq. 4) and r_c for $f'(V_m)$ (in Eq. 4) were presented for individual ion species; K^+, Na^+, Ca^{2+}, and Cl^- fluxes through all channels. These correspond to contributions of rectification in the GHK equations and shift of the reversal potentials due to the change of ion concentrations.

The value dV_L/dt in Eq. 12 is calculated numerically with a time step 0.005 ms. Numerical integration of differential equations of the model was conducted by Euler method with a time step 0.005 ms. When using smaller time steps than 0.005 ms, the results, for practical purposes, remained the same.

RESULTS

As a case study, r_c defined by Eq. 12 was evaluated in various phases of the action potential in the SA node and ventricular cell models. The value I_m includes the following ion channels and ion transporters in the SA node cell model (7),

$$\begin{aligned} I_m = {} & I_{Na} + I_{CaL} + I_{CaT} + I_{st} + I_{ha} + I_{K1} + I_{Kr} + I_{Ks} \\ & + I_{KACh} + I_{Clb} + I_{bNSC} + I_{Cab} + I_{Kpl} + I_{1(Ca)} \\ & + I_{KATP} + I_{NaCa} + I_{NaK} + I_{PMCA}, \end{aligned} \quad (14)$$

and in the ventricular myocyte model (8),

$$\begin{aligned} I_m = {} & I_{Na} + I_{CaL} + I_{CaT} + I_{K1} + I_{Kr} + I_{Ks} + I_{to} + I_{Clb} \\ & + I_{CFTR} + I_{VRCC} + I_{bNSC} + I_{Cab} + I_{Kpl} + I_{1(Ca)} \\ & + I_{KATP} + I_{NaCa} + I_{NaK} + I_{PMCA}, \end{aligned} \quad (15)$$

The definitions of the abbreviations are presented in the legend of Table 1. To facilitate understanding of the results below, the sign of r_c is summarized in Table 2. For example, if an inward current is carried through a channel and the $p(o)$ of the channel increases, this increases dV_L/dt, and makes r_c positive in the depolarization phase ($dV_L/dt > 0$) or negative in the repolarization phase ($dV_L/dt < 0$).

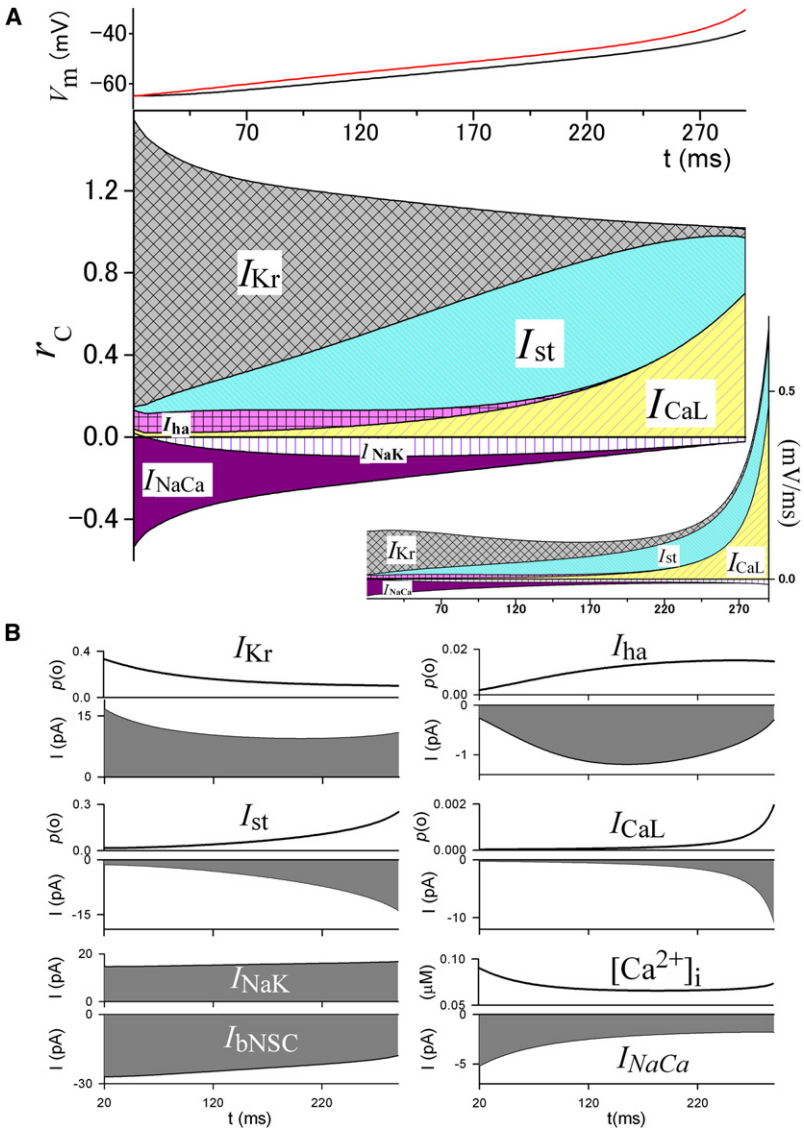

FIGURE 3 Time profile of r_c during slow diastolic depolarization in the SA node model. (*A*) (*Top*) Time-dependent changes of V_L (*red*) and V_m (*black*). These are the same curves as those shown in Fig. 2 *A*. (*Bottom*) Time-dependent changes of r_c of the major current components calculated by Eq. 12. (*Inset*, *right bottom*) The numerators in Eq. 12 for the corresponding currents. (*B*) Changes of $p(o)$ or amplitude of the corresponding currents, and $[Ca^{2+}]_i$. It should be noted that the numerical calculation of r_c has poor precision when dV_L/dt approaches 0 because r_c is normalized with dV_L/dt (the denominator in Eq. 12). Therefore, we excluded the ranges in which dV_L/dt is close to zero from the analyses (also done in Figs. 4 and 5).

Slow diastolic depolarization in SA node cells

Fig. 3 *A* shows r_c for the major currents obtained by fixing $p(o)$ of ion channels, or by fixing the turnover rate of transporters during diastolic depolarization in the SA node cell model. Fig. 3 *B* shows the time-dependent variations of $p(o)$ and the current amplitude. The magnitude of dV_L/dt remained nearly constant at ~0.09 mV/ms during the initial 200 ms after the maximum diastolic potential, and increased exponentially thereafter, as shown in Fig. 3 *A* and the inset in this figure. At the beginning of depolarization, dV_L/dt is largely determined by the deactivation of the outward I_{Kr} (i.e., the decrease in $p(o)$ of I_{Kr}). As r_c of I_{Kr} decreases, it is substituted by those of the inward currents, I_{st} and I_{CaL}, via depolarization-dependent activation. The r_c of I_{st} reached a peak of ~0.63 and then decreased after 220 ms, which is simply biased by the much larger increase in r_c of I_{CaL} (*inset* in Fig. 3). Although I_{CaL} is the main current in the upstroke of the action potential, a tiny increase of $p(o)$ (<0.002) before upstroke also plays a significant role in leading the diastolic depolarization. Inward I_{ha} also plays a positive role at the early stage with an r_c of ~0.1. This is relatively small because the increase of $p(o)$ saturates at ~250 ms and the amplitude of I_{ha} is small. The lead-potential analysis clearly separates the role of I_{bNSC} from that of V_m-gated currents. It has been reported that I_{bNSC}, the largest inward current of ~−25 pA, plays a role in diastolic depolarization by driving V_m toward its reversal potential of ~0 mV (9). However, the r_c of I_{bNSC} is zero because I_{bNSC} is a nongated channel current (i.e., $p(o) = 1$), exclusive of trivial contributions of E_X or $f'(V_m)$. Inward I_{NaCa} has a negative r_c, because the amplitude of I_{NaCa} gradually decreases during the diastolic depolarization period. This decrease of I_{NaCa} is attributable to a decrease of $[Ca^{2+}]_i$ in the first two-thirds of the depolarization phase after the peak reached in the previous

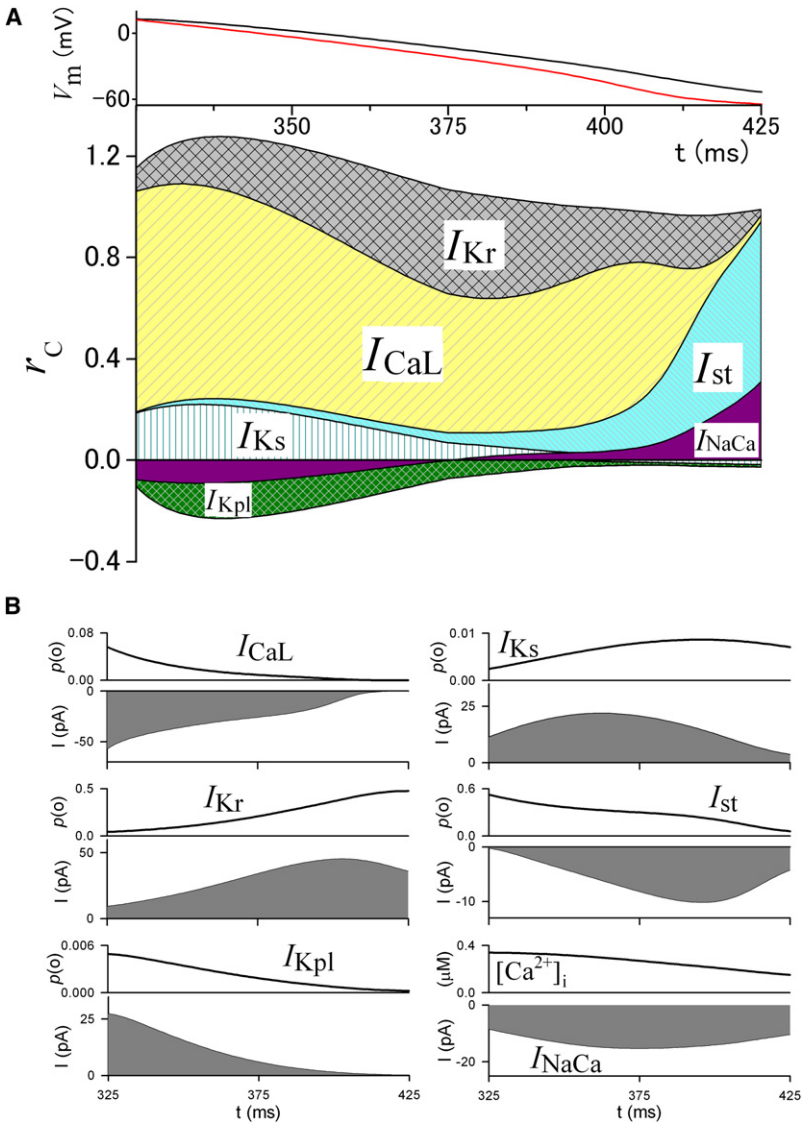

FIGURE 4 Time profile of r_c during repolarization of the SA node action potential. (*A*) (*Top*) Time-dependent changes of V_L (*red*) and V_m (*black*). These are the same curves as those shown in Fig. 2 *A*. (*Bottom*) Time-dependent changes of r_c of the major membrane currents. (*B*) Changes of $p(o)$ or amplitude of the corresponding currents, and $[Ca^{2+}]_i$.

action potential and a continuous increase in V_m. I_{NaK} also has a negative r_c because the outward I_{NaK} increases with depolarizing V_m.

Repolarization of the SA node action potential

Surprisingly, inward I_{CaL} has a larger r_c in driving repolarization than any of the other outward currents (Fig. 4). This effect is attributable to a continuous decrease in $p(o)$ through Ca^{2+}-dependent inactivation during the action potential and also through removal of the voltage-dependent activation in the final rapid repolarization. The $p(o)$ of the outward I_{Kr} continuously increases via fast recovery from inactivation and thereby its r_c is positive throughout the duration of the action potential. I_{Ks} initially has a positive r_c comparable to that of I_{Kr}, and then its r_c gradually decreases because the increase of $p(o)$ becomes slower. I_{st} plays the largest role near the end of repolarization because its activation gate has a dynamic range that is more negative than those for I_{CaL} and I_{Kr}. The monotonic decrease in the $p(o)$ of I_{Kpl} via V_m-dependent rectification interferes with repolarization with r_c ~−0.1. I_{NaCa} also hampers repolarization in the initial half of the repolarization phase with a negative r_c but accelerates repolarization in the latter half because the amplitude of the inward I_{NaCa} initially increases and then decreases.

Repolarization in ventricular myocytes

As in the SA node cells, I_{CaL} is the major current that determines the plateau potential shape with the largest r_c by its time-dependent decrease of the $p(o)$ in the repolarization of the ventricular action potential (Fig. 5). The value r_c of I_{K1} gradually substitutes that of I_{CaL} in the latter half of the plateau, since the $p(o)$ of the outward I_{K1} progressively increases due to release from the Mg^{2+} block. Another

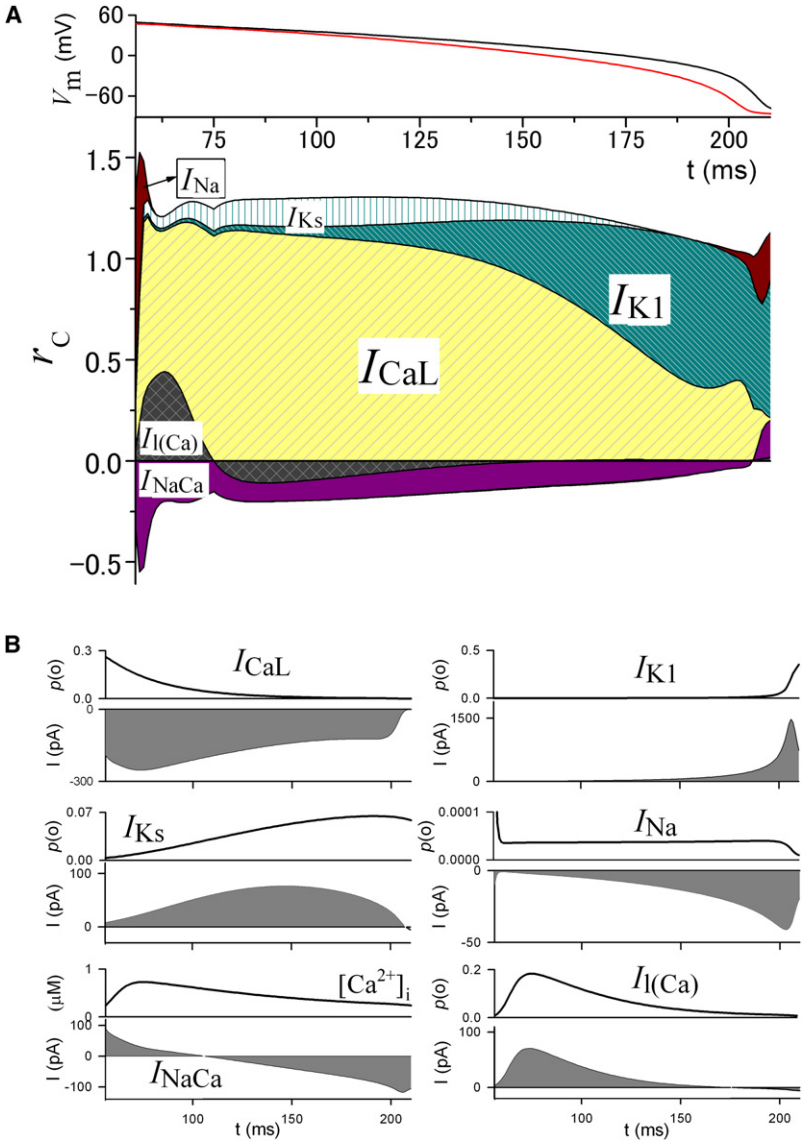

FIGURE 5 The time profile of r_c during repolarization of the ventricular action potential. (*A*) (*Top*) Time-dependent changes of V_L (*red*) and V_m (*black*). These are the same curves as those shown in Fig. 2 *B*. (*Bottom*) Time-dependent changes of r_c of the major membrane currents. (*B*) Changes of $p(o)$ or amplitude of the corresponding currents, and $[Ca^{2+}]_i$.

outward current, I_{Ks}, is responsible for the repolarization during an initial 130 ms (for the repolarization near plateau potential) with r_c of ~0.15 due to the increase of the $p(o)$. The rapid decrease in the $p(o)$ of I_{Na} via inactivation immediately after the upstroke of the action potential plays a major role in phase 1 repolarization. Additionally, the final decrease of the $p(o)$ via deactivation of I_{Na} in phase 3 repolarization is responsible for its positive r_c. Although I_{Na} provides an inward current that progressively increases up to −40 pA, its r_c is invisibly small during the plateau because the $p(o)$ hardly changes, and acts like a background current. The r_c of the outward $I_{l(Ca)}$ is determined by the time course of the intracellular Ca^{2+} transient, as shown in Fig. 5 *B*. The initial rapid increase in $[Ca^{2+}]_i$ increases the $p(o)$ of $I_{l(Ca)}$, resulting in a relatively large r_c during the initial 20 ms followed by a negative r_c due to the decay of $[Ca^{2+}]_i$. The amplitude of I_{NaCa} steadily decreases from outward to inward along the decay time course of $[Ca^{2+}]_i$, and thereby I_{NaCa} has a negative r_c during the plateau, except in the last rapid repolarizing phase. These currents with a negative r_c work to hamper the repolarization. The rest of the currents, such as I_{bNSC}, I_{VRCC}, I_{NaK}, and I_{Kr}, which are not shown in Fig. 5, make minor or no contributions.

DISCUSSION

Major ion channels and electrogenic ion transporters have been identified by both the biochemical and electrophysiological studies of cardiac membrane excitation. The roles of these functional components in generating the spontaneous SA node action potential or autonomic repolarization of ventricular action potentials have been discussed qualitatively based on the dynamic characteristics of the individual current components. The lead-potential analysis developed in our study allows quantification of the relative contribution to the automatic changes in V_m by defining the new concepts

TABLE 1 Average r_c of cellular components

Components	SA node depolarization	SA node repolarization	Ventricular repolarization
p(o) of ion channels			
I_{Na}	0.0009	0.0001	0.0124
I_{CaL}	0.1615	0.5798	0.8729
I_{CaT}	0.0082	0.0008	−0.0003
I_{st}	0.3746	0.1261	—
I_{ha}	0.0520	−0.0038	—
I_{K1}	0.0106	0.0011	0.2419
I_{Kr}	0.5925	0.2673	0.0261
I_{Ks}	0.0186	0.0868	0.0814
I_{to}	—	—	−0.0045
I_{Kpl}	−0.0124	−0.0684	−0.0012
$I_{l(Ca)}$	−0.0047	0.0143	0.0073
I_{KATP}	~0*	~0*	~0*
I_{KACh}	0.0058	0.0151	—
I_{VRCC}	—	—	-0.0008
I_{CFTR}	—	—	0
Turnover rate of transporters			
I_{NaCa}	−0.1519	0.0087	−0.1264
I_{NaK}	−0.0603	−0.0170	−0.0009
I_{PMCA}	0.0040	~0	−0.0012
E_X *and* $f'(V_m)$			
K^+ flux	−0.0050	0.0313	0.0103
Na^+ flux	0.0053	−0.0137	−0.0059
Ca^+ flux	0.0004	−0.0286	−0.1122
Cl^- flux	~0*	~0*	0.0011
Sum	1	1	1

The r_c for $p(o)$ of nongating currents, I_{bNSC}, I_{Clb}, or I_{Cab}, is zero. Abbreviations for currents: I_{Na}, Na^+ current; I_{CaL}, L-type Ca^{2+} current; I_{CaT}, T-type Ca^{2+} current; I_{st}, sustained inward current; I_{ha}, hyperpolarization-activated cation current; I_{K1}, inward rectifier K^+ current; I_{Kr}, delayed rectifier K^+ current, rapid component; I_{Ks}, delayed rectifier K^+ current, slow component; I_{to}, transient outward current; I_{Kpl}, voltage-dependent K^+ current (plateau current); $I_{l(Ca)}$, Ca^{2+}-activated background cation current; I_{KATP}, ATP-sensitive K^+ current; I_{KACh}, Acetylcholine-activated K^+ current; I_{VRCC}, volume-regulated Cl^- channel current; I_{NaCa}, Na^+/Ca^{2+} exchange current; I_{NaK}, Na^+/K^+ pump current; I_{PMCA}, plasma membrane Ca^{2+}-ATPase current; I_{bNSC}, background nonselective cation current; I_{Clb}, background Cl^- current; I_{Cab}, background Ca^{2+} current; I_{CFTR}, cystic fibrosis transmembrane conductance regulator (CFTR) Cl^- channel current.
*$r_c < 10^{-4}$.

of V_L (Eq. 8) and r_c (Eq. 12). This is the first method, to our knowledge, to enable estimation of the negative, as well as the positive, contributions along the time course of V_m. In addition, the contribution of the $p(o)$ of each ion channel can be considered separately from those of rectification in the GHK equation and the change of ion concentrations (r_c of E_X and $f'(V_m)$ in Table 1). In the case studies in the SA node and ventricular cell models, the r_c value of E_X and $f'(V_m)$ was much smaller than that of the $p(o)$ of ion channels. Thus, the selection of an Ohmic (Eq. 2) or a GHK equation (Eq. 3) for describing ion flux may not be critical for considering the r_c in mathematical cell models.

Comparison with other methods of analyzing membrane excitation

A variety of methods have been applied to analyze the mechanisms underlying membrane excitation in mathematical cell models. In this section, lead-potential analysis is compared with previous methods. The most common approaches are inhibition methods, in which a selected ionic current is excluded or decreased in amplitude and consequent changes in membrane excitation are analyzed (10,11). This method is simple, but interpretation of the results is complicated and often somewhat equivocal, because not only the selected current but also other currents are secondarily affected by modification of the action potential or ion concentrations. Furthermore, the nonlinear behavior of the system prevents quantitative estimation of the contribution of each current. Sensitivity analysis can overcome these difficulties by measuring modifications induced by an infinitesimal change of a parameter of interest (i.e., a partial derivative) (5,6). We regard lead-potential analysis as a type of sensitivity analysis because Eq. 12 can be rewritten using the partial derivative of V_L with respect to a fixed component (x; $p(o)$, E_X, $f'(V_m)$, and I_Y):

$$r_c = \frac{\partial V_L}{\partial x} \times \frac{\dot{x}}{\dot{V}_L}. \quad (16)$$

Compared to sensitivity analysis, r_c can be directly interpreted as contribution to automaticity, because the partial derivative of V_L is weighted by $\dot{x}$, the actual change of x at a given moment. $1/\dot{V}_L$ is merely multiplied for normalization.

Bifurcation analysis is also commonly used to analyze the relationships between functional components and membrane excitability. This approach surveys equilibrium points in parameter space (bifurcation diagram) and determines critical values at which bifurcations occur. Bifurcation analyses have been successfully applied to systems with macroscopic modal changes in the V_m dynamics, such as extinction of spontaneous pacemaking in the SA node cell (3), induction of reentrant arrhythmias or ectopic beats in cardiac muscles (2), abnormal initiation of spontaneous

TABLE 2 Polarity of r_c

Action potential phase	Direction of current	Channel		Transporter	
		$dp(o)/dt > 0$	$dp(o)/dt < 0$	$dI_Y/dt > 0$	$dI_Y/dt < 0$
$dV_L/dt > 0$ (depolarization)	Inward	+	−	−	+
	Outward	−	+		
$dV_L/dt < 0$ (repolarization)	Inward	−	+	+	−
	Outward	+	−		

oscillatory firing in ventricular myocytes (4), and repetitive trains of action potentials in muscle fiber (1). Thus, bifurcation analysis is useful for examination of behavioral responses on the level of the entire system with respect to time-independent parameters such as maximum conductance of a channel. Bifurcation analysis qualitatively interprets the results based on topological changes in bifurcation diagrams and, as simplification is required to make the problems manageable, the conclusions from bifurcation diagrams are valid under a specific condition only. On the other hand, lead-potential analysis can be used to clarify the ionic mechanisms in a selected phase of membrane excitation, and provides quantitative measures of the contributions of time-dependent variables of individual ion channels or transporters to the automatic movement of V_m. Furthermore, in its application, simplification is not required for a complicated electrophysiological cell model. Since these two methods integrate information in different respects, we consider that they are complementary for obtaining a comprehensive understanding of the ionic mechanisms underlying membrane excitation.

Comparison with the previous lead-potential method

Lead-potential analysis was first introduced by Sarai et al. (12) to evaluate the contribution of individual current components to slow diastolic depolarization in the SA node model. The new method differs from the previous method in two ways: the equation for V_L and the method of estimating the contribution of ion channels and transporters. First, V_L in the earlier work was defined by the equation

$$V_L = \frac{(G_K E_K + G_{Na} E_{Na} + G_{Ca} E_{Ca} - I_{NaK})}{(G_K + G_{Na} + G_{Ca})}, \quad (17)$$

where G_K, G_{Na}, and G_{Ca} are the whole cell conductances for the net currents $I_{net,K}$, $I_{net,Na}$, and $I_{net,Ca}$, respectively, after excluding I_{NaK}, which is generated by the active transporter. Na^+ and Ca^{2+} components of I_{NaCa} were included in $I_{net,Na}$ and $I_{net,Ca}$, respectively, as I_{NaCa} is driven passively by the electrochemical driving force. Neglecting the fact that several currents were described with the nonlinear GHK equation, the whole cell conductances were approximated by the following Ohmic equations:

$$G_K = (I_{net,K} + 2I_{NaK})/(V_m - E_K), \quad (18)$$

$$G_{Na} = (I_{net,\,Na} - 3I_{NaK})/(V_m - E_{Na}), \quad (19)$$

$$G_{Ca} = I_{net,\,Ca}/(V_m - E_{Ca}). \quad (20)$$

Fig. 6 *A* compares the old V_L calculated with Eq. 17 (*blue curve*) with the new V_L calculated with Eq. 8 (*red curve*) in the guinea-pig SA node model (7) after adding the passive I_{Clb} and the active I_{PMCA} to Eq. 17. The two curves differ because the rectification given by the GHK equation was neglected in the previous study, thereby the old V_L cannot be used for quantitative estimation of the contributions of individual ion channels and transporters. Indeed, the two curves become identical in a model in which all the channel currents are described with Ohmic equations.

In contrast to continuous estimation of dV_L/dt by fixing a component at every moment in the new method, the time-dependent change was fixed throughout the slow diastolic depolarization in the previous lead-potential analysis. In Fig. 6 *B*, the value of $p(o)$ for I_{Kr} or I_{ha} determined at the maximum diastolic potential was used for the next 250 ms to observe the modification of V_L. Comparison of the modified time course of V_L with the control suggested that deactivation of I_{Kr} plays the major role in driving slow diastolic depolarization. However, this conclusion is still qualitative. In contrast, the new lead-potential analysis provides temporal profiles of the contributions and successfully shows the ionic mechanisms of slow diastolic depolarization when taken together with the profile of $p(o)$ and the current size (Figs. 3 *B*, 4 *B*, and 5 *B*).

Limitations and applications of lead-potential analysis

Equation 8 for V_L in Methods includes the assumption that an ion transporter acts like a current source. It should be noted that this assumption might cause an error in the calculation of the lead potential because any responses of transporter currents to changes in electrochemical driving force are ignored. An alternative description might be a linear equation with V_m for its ion driving force, like a channel current. For

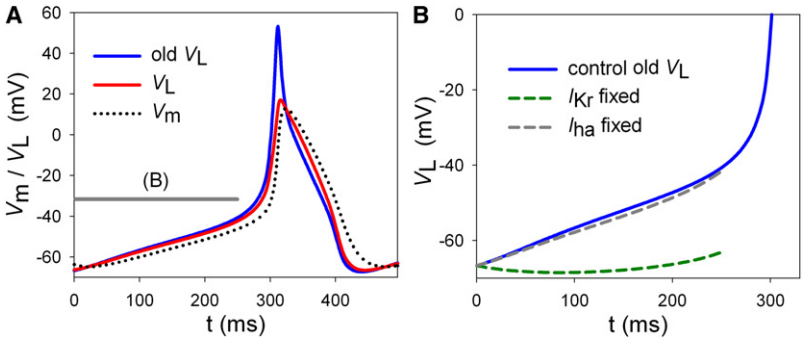

FIGURE 6 Comparison of V_L determined by Eq. 8 (*red solid*) with the old V_L determined by Eq. 17 (*blue solid*). (*A*) Both V_L values meet with V_m (*black dotted*) at $dV_m/dt = 0$. The curves for the present V_L and V_m are the same as those shown in Fig. 2. The gray bars indicate the time spans analyzed in panel *B*. (*B*) Modified time courses of V_L after fixing of I_{Kr} (*green dashed*) or I_{ha} (*gray dashed*). The V_L (*blue*) curve is the same as the blue curve in panel *A*.

example, when I_{NaK} is expressed by a steady-state equation as in many cellular models (10,13), the conductance of the NaK pump, G_{NaK}, might be calculated as

$$G_{NaK} = I_{NaK}/(V_m - E_{NaK}), \quad (21)$$

where E_{NaK}, the reversal potential of I_{NaK}, is given as

$$E_{NaK} = 3E_{Na} - 2E_K + \Delta G_{MgATP}/F. \quad (22)$$

E_{Na} and E_K are the Nernst equilibrium potential and ΔG_{MgATP} is the free energy change by hydrolysis of ATP. In this case, G_{NaK} is included in the total conductance of a cell as for channels, and Eq. 8 should also be modified with Eq. 21. However, G_{NaK} is hard to define with Eq. 21 when I_{NaK} is generated by multiple states-transitions, as in the Kyoto model. G_{NaK} is closely linked to I_{NaK} because the transport of ions necessarily causes the rearrangement of the state distribution. Therefore, transporter currents generated by states-transitions cannot be expressed with a battery and a conductance like a channel current. Thus, we treated a transporter current as a current source for simplicity in this study.

The selection of components to fix in the lead-potential analysis is dependent on the questions in a study, and the minimum constraint is that Eq. 13 should be satisfied for all the fixed components. For example, I_{CaL} is usually described by V_m-gated activation, inactivation, and Ca^{2+}-dependent inactivation. In addition, I_{CaL} is known to be affected by $[ATP]_i$. The model equation of I_{CaL} can be expressed as

$$\begin{aligned} I_{CaL} &= p_{CaL}p(o)f(V_m) \\ &= p_{CaL}\, d\, f\, f_{Ca}\, h([ATP]_i)\cdot f(V_m) \end{aligned}, \quad (23)$$

where

$$\frac{dd}{dt} = i(V_m),\ \frac{df}{dt} = j(V_m),\ \frac{df_{Ca}}{dt} = k([Ca^{2+}]_i), \quad (24)$$

$$h([ATP]_i) = 1/(1 + K_{ATP}/[ATP]_i^n), \quad (25)$$

and $f(V_m)$ is the nonlinear part of the GHK equation as in Eq. 3. In this case, r_c may be calculated for individual terms, d, f, f_{Ca}, and $[ATP]_i$, instead of $p(o)$. However, V_m or $[Ca^{2+}]_i$ inside of i, j, or k in Eq. 24 should not be fixed instead of d, f, and f_{Ca}, which are determined by state transitions.

Several types of models have been published for cardiac membrane excitation. However, it is difficult to assess the different models by comparing simulation results with corresponding experimental findings, such as the action potential shape, voltage-clamp recordings of the whole cell as well as individual current components, or the responses of the model to various kinds of perturbations. The comparison becomes even more difficult when different models show similar behavior but with distinct mechanisms. Lead-potential analysis may provide additional clues to assess the relevance of models by analyzing the underlying mechanisms in individual cell models.

In this study, we introduced a new analytic method to quantify the contributions of the cellular components to automaticity of V_m, with application of the method to cardiac membrane excitation. Since Eqs. 1–12 include no assumption specific for cardiac membrane excitation, the new method of lead-potential analysis may be generally applied to different cell types to clarify the ionic mechanisms underlying automatic membrane potential changes.

This work was supported by Ritsumeikan-Global Innovation Research Organization at Ritsumeikan University and the Biomedical Cluster Kansai project of the Ministry of Education, Culture, Sports, Science, and Technology of Japan.

REFERENCES

1. Cannon, S. C., R. H. Brown, Jr., and D. P. Corey. 1993. Theoretical reconstruction of myotonia and paralysis caused by incomplete inactivation of sodium channels. *Biophys. J.* 65:270–288.
2. Chay, T. R., and Y. S. Lee. 1992. Studies on re-entrant arrhythmias and ectopic beats in excitable tissues by bifurcation analyses. *J. Theor. Biol.* 155:137–171.
3. Kurata, Y., I. Hisatome, S. Imanishi, and T. Shibamoto. 2003. Roles of L-type Ca^{2+} and delayed-rectifier K^+ currents in sinoatrial node pacemaking: insights from stability and bifurcation analyses of a mathematical model. *Am. J. Physiol. Heart Circ. Physiol.* 285:H2804–H2819.
4. Kurata, Y., I. Hisatome, H. Matsuda, and T. Shibamoto. 2005. Dynamical mechanisms of pacemaker generation in IK1-downregulated human ventricular myocytes: insights from bifurcation analyses of a mathematical model. *Biophys. J.* 89:2865–2887.
5. Kim, T. H., S. Y. Shin, S. M. Choo, and K. H. Cho. 2008. Dynamical analysis of the calcium signaling pathway in cardiac myocytes based on logarithmic sensitivity analysis. *Biotechnol. J.* 3:639–647.
6. Weaver, C. M., and S. L. Wearne. 2008. Neuronal firing sensitivity to morphologic and active membrane parameters. *PLOS Comput. Biol.* 4:e11.
7. Himeno, Y., N. Sarai, S. Matsuoka, and A. Noma. 2008. Ionic mechanisms underlying the positive chronotropy induced by β1-adrenergic stimulation in guinea pig sinoatrial node cells: a simulation study. *J. Physiol. Sci.* 58:53–65.
8. Takeuchi, A., S. Tatsumi, N. Sarai, K. Terashima, S. Matsuoka, et al. 2006. Ionic mechanisms of cardiac cell swelling induced by blocking Na^+/K^+ pump as revealed by experiments and simulation. *J. Gen. Physiol.* 128:495–507.
9. Dokos, S., B. Celler, and N. Lovell. 1996. Ion currents underlying sinoatrial node pacemaker activity: a new single cell mathematical model. *J. Theor. Biol.* 181:245–272.
10. Demir, S. S., J. W. Clark, C. R. Murphey, and W. R. Giles. 1994. A mathematical model of a rabbit sinoatrial node cell. *Am. J. Physiol.* 266:C832–C852.
11. Zhang, H., A. V. Holden, I. Kodama, H. Honjo, M. Lei, et al. 2000. Mathematical models of action potentials in the periphery and center of the rabbit sinoatrial node. *Am. J. Physiol. Heart Circ. Physiol.* 279:H397–H421.
12. Sarai, N., S. Matsuoka, S. Kuratomi, K. Ono, and A. Noma. 2003. Role of individual ionic current systems in the SA node hypothesized by a model study. *Jpn. J. Physiol.* 53:125–134.
13. Rice, J. J., M. S. Jafri, and R. L. Winslow. 2000. Modeling short-term interval-force relations in cardiac muscle. *Am. J. Physiol. Heart Circ. Physiol.* 278:H913–H931.